Dynamics of Multifunctional Polyhedral Oligomeric Silsesquioxane/ Poly(propylene oxide) Nanocomposites As Studied by Dielectric Relaxation Spectroscopy and Dynamic Mechanical Spectroscopy

Yu Bian, Srdjan Pejanović,[‡] Jose Kenny,[§] and Jovan Mijović*,[†]

Othmer-Jacobs Department of Chemical and Biological Engineering, Polytechnic University, Six Metrotech Center, Brooklyn, New York 11201; Department of Chemical Engineering, Faculty of Technology, University of Belgrade, Karnegijeva 4, Belgrade 11000, Serbia; and Department of Materials Science and Technology, University of Perugia, Terni 05100, Italy

Received February 15, 2007; Revised Manuscript Received June 19, 2007

ABSTRACT: An investigation was carried out of the segmental and normal mode dynamics in multifunctional polyhedral oligomeric silsesquioxane (POSS)/poly(propylene oxide) (PPO) nanocomposites. Data were generated by broadband dielectric relaxation spectroscopy (DRS) and dynamic mechanical spectroscopy (DMS) over a wide range of frequency and temperature. Neat PPO exhibits two relaxation processes: normal mode (α_N) and segmental mode (α). The two multifunctional POSS reagents utilized (octaglycidyldimethylsilyl-POSS and octaepoxycyclohexyldimethylsilyl-POSS) show a segmental process at lower frequency and a local relaxation at higher frequency. The POSS/PPO nanocomposites also show two relaxation processes (α_N and α), but interestingly, their time scale is shorter than in the corresponding neat PPO. Molecular origin and spectral characteristics of all relaxations are described. Comparison of DRS and DMS results revealed identical trends with respect to the POSS concentration, temperature, and the same time scale for the segmental and normal mode process. A detailed account of the effect of structure, concentration, and dispersion of POSS, molecular weight of PPO, and temperature on the molecular origin, temperature dependence, and spectral characteristics of relaxation processes in POSS/PPO nanocomposites is provided.

Introduction

The development of inorganic-nanoparticle/polymer-matrix nanocomposites has attracted considerable attention in recent years.[1−3] Among various nanoparticles, polyhedral oligomeric silsesquioxanes (POSS) are particularly attractive because of their unique structure.[4−6] POSS molecules consist of a rigid silica core with different organic moieties covalently bonded to the silicon atoms.[7−9] The wide variety of functional moieties that can be affixed to silicon and their nanoscopic dimensions make POSS molecules attractive candidates for a wide range of application. One example is the field of nanocomposites, where a judicious selection of functional moieties may improve dispersion of POSS in the polymer matrix,[10−17] enhance processing characteristics,[18] and impart desired physical and mechanical properties. The end group on a functional moiety may be nonreactive or it may react with the polymer matrix. Nonreactive end groups enhance dispersion and properties of POSS/polymer blends,[19−31] while reactive end groups may lead to the formation of copolymers[32−39] or networks.[40−55]

Nonreactive POSS/polymer nanocomposites have been investigated with several techniques, and improvements of their bulk properties, such as thermal stability,[24] glass transition temperature,[23,25,26] and mechanical performance,[27] have been reported. What is missing, however, is information about the molecular motions that underlie physical and mechanical response.

The knowledge of dynamics on the nanoscopic and microscopic level is crucial for understanding the time scales and length scale of molecular motions that underlie the macroscopic or bulk behavior. But information on dynamics of nonreactive POSS/polymer nanocomposites is scarce. A few reported studies utilized dynamic mechanical measurements[28−31] to investigate nanocomposites with POSS concentration below 10 wt % that include cyclohexyl-POSS/poly(methyl methacrylate)s (PMMA), isobutyl-POSS/PMMA,[28] methyl-POSS/ethylene−propylene copolymers (EP),[29] methyl-POSS/polyethylene (PE),[30] and cyclopentyl-POSS/PE.[31] A common finding in those studies regards the morphology of nanocomposites: POSS molecules are dispersed in the polymer matrix below threshold concentration that defines the solubility limit and form aggregates above that value. The viscoelastic behavior of these nanocomposites is determined by the chemical and physical properties of the matrix and POSS molecules as well as the interactions betweens these two components.

The principal objective of this study is to conduct an investigation of the fundamental dynamic features of multifunctional nonreactive POSS/PPO nanocomposites. Specifically, we employ dielectric relaxation spectroscopy (DRS) and dynamic mechanical spectroscopy (DMS) to investigate the effect on dynamics of *molecular variables*, such as the type, concentration, and architecture of nanoparticles and molecular weight of polymer, and *external variable*, such as temperature and frequency. To the best of our knowledge, this study marks the first time that DRS was used to investigate the dynamics of POSS/polymer nanocomposites and DRS and DMS spectra were compared.

Experimental Section

A. Materials. Polymer. Linear poly(propylene oxide) (PPO) with symmetrical dipole inversion was used in this study, and its structure is shown in Figure 1. Two arms emanate from a central point, each containing an uninverted dipole sequence. This polymer has type

* To whom correspondence should be addressed. E-mail: jmijovic@poly.edu.
[†] Polytechnic University.
[‡] University of Belgrade.
[§] University of Perugia.

10.1021/ma0704109 CCC: $37.00
Published on Web 07/28/2007

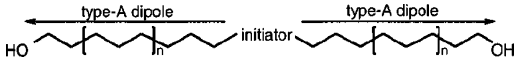

Figure 1. PPO architecture (linear PPO chain with symmetrically inverted dipoles).

A dipoles[56−59] parallel to the polymer backbone, which relax via the normal mode process (α_N process), and the transverse dipole moment component, which relaxes via the segmental process (α process). Three PPOs with molecular weights of 2 kg/mol (PPO2K), 4 kg/mol (PPO4K), and 8 kg/mol (PPO8K) were obtained from Bayer.

DGEBA (diglycidyl ether of bisphenol A), with molecular weight of 374 g/mol, was obtained from Aldrich.

Multifunctional POSS. Multifunctional POSS monomers possess a hybrid inorganic−organic three-dimensional structure and contain eight reactive organic functional groups, as shown in Figure 2. The dimension of POSS cubic frame is around 1.2−1.5 nm. Two different multifunctional POSS monomers were selected for study: octaglycidyldimethylsilyl-POSS [OG], shown in Figure 2A, and octaepoxycyclohexyldimethylsilyl-POSS [OC], shown in Figure 2B. The side groups are different in OG and OC, although each monomer contains a terminal epoxy group. Specifically they differ in that the end-group epoxy is attached to a linear glycidyl moiety in OG and to a cyclohexyl ring in OC. At room temperature, OG is a liquid with a viscosity of 300 cP, while OC is a solid. These two POSS monomers were selected for study in order to elucidate the effect of side-chain structure on dynamics. POSS monomers were obtained from Hybrid Plastic.

POSS/PPO Nanocomposites. Desired amounts of POSS and PPO were mixed in toluene using a high-speed stirrer. Toluene evaporates fast, and good dispersions of POSS in PPO are obtained. All mixtures were degassed prior to measurements.

Throughout the text, the concentration of POSS in the nanocomposites is defined as the ratio of the number of OH groups in the PPO and the number of reactive functional chains in POSS according to eq 1:

$$N = \frac{\text{number of OH in PPO}}{\text{number of reactive functional chains in POSS}} \qquad (1)$$

Note that POSS concentration increases with decreasing N. The characteristics of the samples investigated are summarized in Table 1. In the sample codes used for nanocomposites, the first two letters define the type of POSS (OG or OC) and the third one, "P", stands for PPO. The number that follows (K) defines the molecular weight of PPO (kg/mol), and the final number describes the parameter N defined above. For example, OCP4K-1 represents a nanocomposites of POSS (OC) and PPO (P) with molecular weight of 4000 g/mol (4K) at ratio N equal to one (1). The sample codes are also listed in Table 1.

B. Techniques. Dielectric Relaxation Spectroscopy (DRS). Our facility combines commercial and custom-made instruments that include (1) Novocontrol α high-resolution dielectric analyzer (3 μHz−10 MHz) and (2) Hewlett-Packard 4291B rf impedance analyzer (1 MHz−1.8 GHz). Both instruments are interfaced to computers and equipped with heating/cooling controls, including the Novocool system custom-modified for measurements over the entire frequency range from 3 μHz to 1.8 GHz. The samples were placed between the stainless steel electrodes (we obtained identical results using aluminum electrodes). The diameter of the electrodes is 12 mm, and the sample thickness is 0.05 mm. Further details of our DRS facility are given elsewhere.[60−62]

Dynamic Mechanical Spectroscopy (DMS). Experiments were conducted using a Rheometric Scientific's Advanced Rheometric Expansion System (ARES) rheometer. Measurements were performed in the frequency range from 0.001 to 100 rad/s. Parallel plate configuration was employed with a typical gap between the plates of 0.5−1.5 mm. Strain values were adjusted from 0.2 to 25% for the measurable torque in the linear viscoelastic range.

Optical Microscopy (OM). A Nikon HFX-II optical microscope was used to investigate the dispersion and aggregation of POSS nanoparticles in the polymer matrix at room temperature.

Differential Scanning Calorimetry (DSC). A TA Instruments Co. DSC model 2920 was used. Samples were placed in sealed DSC pans and scanned at a heating or cooling rate of 10 °C/min.

Results and Discussion

1. Individual Components: Poly(propylene oxide) (PPO). The background on the dielectric properties of polymers and other glass formers has been described in great detail in a number of books and key reviews.[63−65] DRS studies of neat PPO have also been reported,[66,67] and hence our goal here is not to be comprehensive. The glass transition temperature of neat PPO is not a function of molecular weight ($T_g = -68$ °C as measured by DSC). The experimentally obtained dielectric spectra were deconvoluted using a sum of the well-known Havriliak−Negami (HN) functional form[68] and the conductivity term:

$$\epsilon^*(\omega) = \epsilon' - i\epsilon'' = \sum_{k=1}^{n}\left[\epsilon_{\infty k} + \frac{\epsilon_{0k} - \epsilon_{\infty k}}{(1 + (i\omega\tau_k)^{a_k})^{b_k}}\right] - i\left(\frac{\sigma}{\omega\epsilon_v}\right)^N \qquad (2)$$

where a_k and b_k are the shape parameters that define the breadth and the symmetry of the spectrum, respectively, σ is the conductivity, ϵ_v is the vacuum permittivity, and τ_k is the average relaxation time obtained from the fits. The HN function reduces to the Debye equation when $a = b = 1$ and the Cole−Cole equation when $b = 1$.[69] The temperature dependence of the relaxation time for the segmental (τ_S) and normal (τ_N) mode

Table 1. OG/PPO and OC/PPO Nanocomposites Investigated

description	N	POSS (mol)	PPO (mol)	wt % of POSS in PPO matrix (OG/OC)	code
OG/OC +PPO2K	8	1.00	32.00	2.5/2.7	OGP/OCP 2K-8
OG/OC +PPO2K	4	1.00	16.00	4.9/5.4	OGP/OCP 2K-4
OG/OC +PPO2K	2	1.00	8.00	9.4/10.3	OGP/OCP 2K-2
OG/OC +PPO2K	1	1.00	4.00	17.1/18.6	OGP/OCP 2K-1
OG/OC +PPO2K	0.5	1.00	2.00	29.2/31.4	OGP/OCP 2K-05
OG /OC +PPO2K	0.25	1.00	1.00	45.3/47.8	OGP/OCP 2K-025
OG /OC +PPO4K	4	1.00	16.00	2.6/2.9	OGP/OCP 4K-4
OG /OC +PPO4K	2	1.00	8.00	5.1/5.6	OGP/OCP 4K-2
OG /OC +PPO4K	1	1.00	4.00	9.7/10.7	OGP/OCP 4K-1
OG /OC +PPO4K	0.5	1.00	2.00	17.8/19.3	OGP/OCP 4K-05
OG /OC +PPO4K	0.25	1.00	1.00	30.2/32.4	OGP/OCP 4K-025
OG /OC +PPO4K	0.125	1.00	0.50	46.4/48.9	OGP/OCP 4K-0125
OG /OC +PPO8K	2	1.00	8.00	2.7/2.9	OGP/OCP 8K-2
OG /OC +PPO8K	1	1.00	4.00	5.3/5.8	OGP/OCP 8K-1
OG /OC +PPO8K	0.5	1.00	2.00	9.8/10.9	OGP/OCP 8K-05
OG /OC +PPO8K	0.25	1.00	1.00	18.2/19.7	OGP/OCP 8K-025
OG /OC +PPO8K	0.125	1.00	0.50	30.7/32.9	OGP/OCP 8K-0125

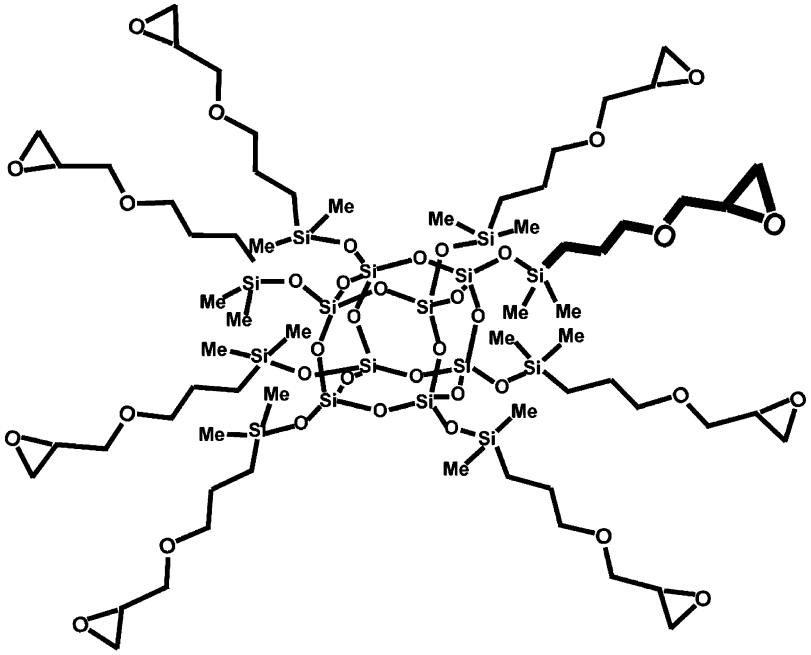

A. OctaGlycidyldimethylsilyl-POSS (OG)

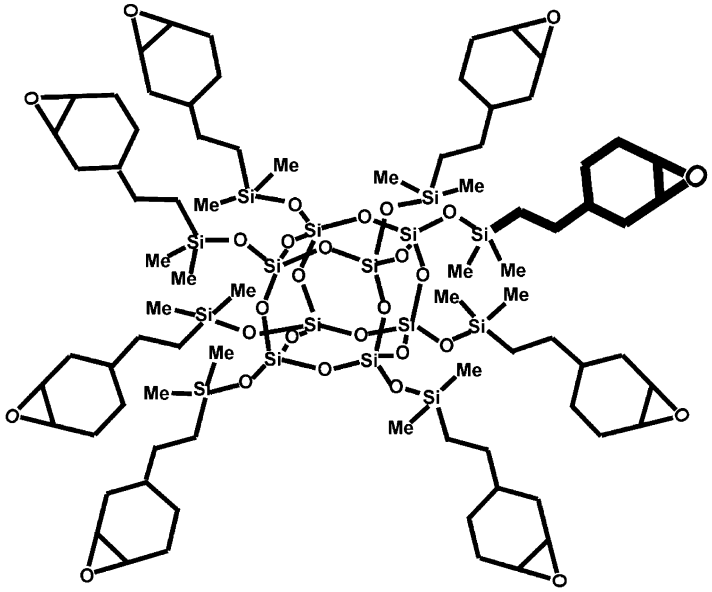

B. OctaEpoxyCyclohexyldimethylsilyl-POSS (OC)

Figure 2. Chemical structure of multifunctional POSS monomers.

processes confirms that the increase in molecular weight slows down the normal mode process but does not affect the segmental process. The temperature dependence of the average relaxation time for both processes is of the Vogel−Fulcher−Tammann (VFT) type[63−65] described by

$$\tau = \tau_0 \exp\left(\frac{B}{T - T_v}\right) \tag{3}$$

Further details of the dynamics of neat PPO have been given elsewhere.[66,67]

OG and OC. We begin the analysis of OG and OC dynamics by first describing their individual DRS spectra and seeking to elucidate the molecular origin of the observed relaxations. Dielectric loss of OG in the frequency domain with temperature as a variable is shown in Figure 3. Dielectric permittivity is shown in the inset in Figure 3. OG shows two processes in the frequency range between 10^{-2} and 10^{8} Hz and at temperatures between −100 and −40 °C. These two processes possess the characteristics of α relaxation (lower frequency process) and β relaxation (higher frequency process) in glass formers.

DRS spectra of OC are quite different as evident from Figure 4, which shows dielectric loss in the frequency domain with temperature as a variable. These spectra were generated in the frequency range between 10^{-2} and 10^{6} Hz and in the temperature range between −100 and 100 °C. At −100 °C (filled squares) OC shows a β process, centered at 3×10^{4} Hz, that shifts to higher frequency with increasing temperature and exits our frequency window at −50 °C. In the temperature range between

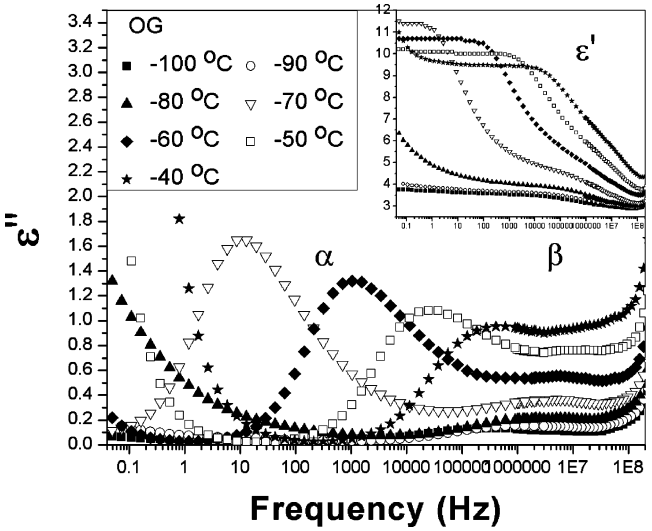

Figure 3. Dielectric loss and permittivity (inset) of OG in the frequency domain with temperature as a parameter.

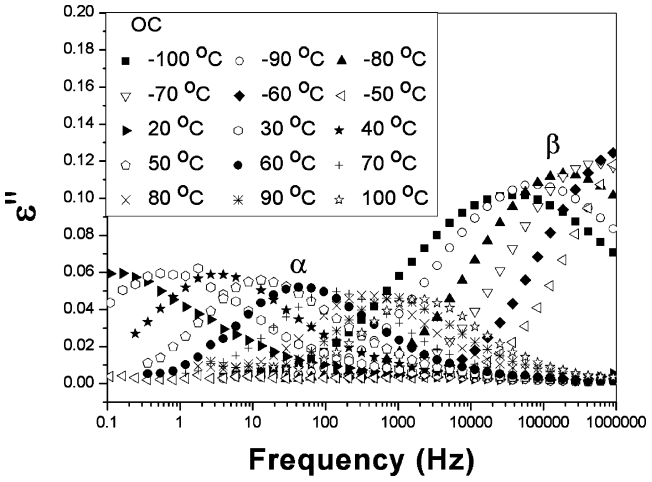

Figure 4. Dielectric loss of OC in the frequency domain with temperature as a parameter.

−40 and 10 °C, we observe no relaxation processes at frequencies between10^{-2} and 10^6 Hz. With further increase in temperature, at about 20 °C, the α process enters the low-frequency end of the spectrum. The α process shifts to higher frequency and decreases in intensity with further increase in temperature.

A direct comparison of the OG and OC spectra reveals some common features: (1) both OG and OC undergo two relaxation processes (α and β), (2) all processes shift to higher frequency with increasing temperature, and (3) dielectric strength decreases for the α process and increases for the β process with increasing temperature. But the differences between OG and OC dynamics are notable. For example, the dielectric strength of the α process in OC is considerably lower than in OG at the same temperature.

The temperature dependence of the average relaxation time for each process in OG and OC (obtained from the HN fits) was determined, and the results are plotted in Figure 5 (solid lines are fits). Also included in Figure 5 is the temperature dependence of the average relaxation time for α and β processes in diglycidyl ether of Bisphenol A (DGEBA), a widely used bifunctional epoxy resin. This comparison is interesting because DGEBA has terminal glycidyl groups (like OG), and its dynamics have been investigated before by DRS.[70,71] We note that the calorimetric (DSC) glass transition temperature (T_g) is −78 °C for OG and −18 °C for DGEBA. OC shows a weak

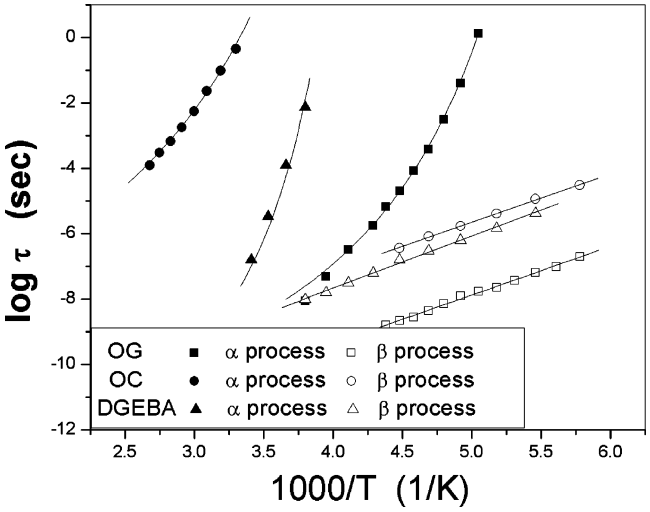

Figure 5. Temperature dependence of the average relaxation time for α and β processes in OG, OC, and DGEBA.

Table 2. VFT Parameters for the Segmental Process in OG, OC, and DGEBA

	segmental process		
material	τ_0 (s)	B (10^3)	T_v (K)
OG	5.7×10^{-13}	1114	159
OC	5.6×10^{-10}	2209	197
DGEBA	1.0×10^{-14}	1148	222

glass transition at −7 °C and a melting point at 125 °C. The temperature dependence of the average relaxation time follows the Vogel−Fulcher−Tammann (VFT) form for the α process and the Arrhenius form for the β process in all compounds. The corresponding VFT parameters are listed in Table 2. The time scales of α and β relaxations in OG are much shorter than in OC.

The molecular origin of these processes is considered next. There is little doubt that the α process in OG and OC results from the segmental motions of the side chains of POSS. The lower dielectric strength of the α process in OC vs OG is the consequence of the lower concentration of mobile dipoles in the amorphous region, while the longer time scale is due to the higher T_g. The β process originates from the local motions and is slower in OC than OG because of the increased rigidity of side chains due to the incorporation of the cyclohexyl ring. DGEBA also shows two processes in the temperature range between −100 and 100 °C, identified as segmental (α) and local (β), respectively. Figure 5 shows that the average relaxation time for the β process in DGEBA is closer to that of OC while the average relaxation time for the α process falls between those of OG and OC. DGEBA and OG have the same terminal glycidyl groups, but OG side chains are more flexible, resulting in the lower glass transition temperature. The T_g of OC is higher than that of DGEBA and OG, and hence the time scale of the α process in these three compounds expressed by the average relaxation time for segmental motions (τ_S) is as follows: $\tau_{S-OC} > \tau_{S-DGEBA} > \tau_{S-OG}$. The β process has similar activation energy in all three compounds (ca. 29 kJ/mol), suggesting the same molecular origin.

2. POSS/PPO Nanocomposites. (a) Optical Microscopy and Thermal Analysis. The effect of OC concentration (6 and 30 wt %) and PPO molecular weight (MW = 2K, 4K, and 8K g/mol) on the extent of dispersion in OCP nanocomposites was investigated first by optical microscopy (Figure 6). OC dissolves in the PPO matrix below 2.5 wt %, and the resulting systems is transparent (not shown here).With increasing concentration, the

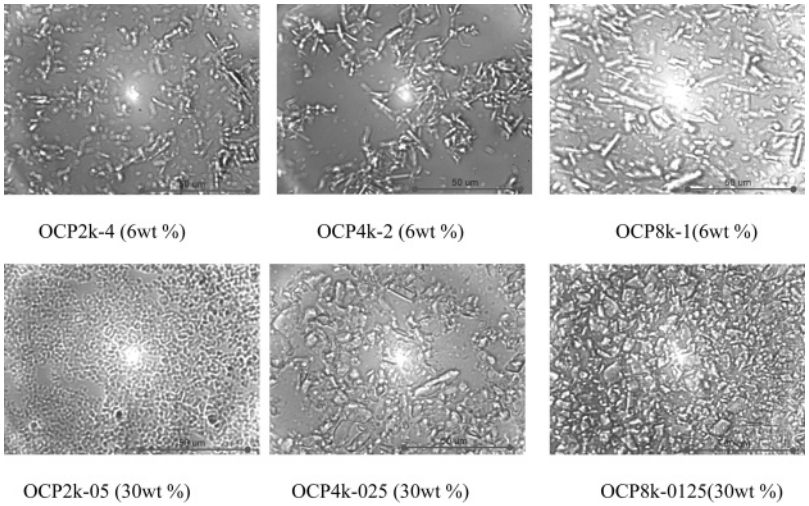

Figure 6. Morphology of OCP nanocomposites with molecular weight of PPO and OC concentration as parameters.

formation of needlelike aggregates is observed as seen in Figure 6A. The size of OC aggregates at a given concentration increases with increasing molecular weight of PPO as evident by examining Figure 6A,B from left to right. By comparing parts A and B of Figure 6 vertically, we see that the effect of molecular weight on aggregation is more pronounced at higher OC concentration (30 wt %). All nanocomposites were stable for at least 1 month, and all DRS and DMS experiments were performed within that time frame. We recall that OG is a transparent liquid, and hence no attempts were made to study the morphology of OGP nanocomposites by optical microscopy.

The following results were obtained from the thermal analysis of nanocomposites. The DSC glass transition temperature of OCP nanocomposites is −68 °C and is not affected by the OC concentration. The melting point in OCP nanocomposites is observed at lower temperature (112 °C for OCP4K-0125) in comparison with the neat OC (125 °C). The glass transition temperature of OGP nanocomposites decreases with increasing OG concentration according to the law of mixtures. OGP nanocomposites are wholly amorphous and do not have a melting point.

(b) Dielectric Relaxation Spectroscopy (DRS). In this section, we describe the results of DRS measurements of OGP and OCP nanocomposites. The key parameters that define the dynamics of nanocomposites are discussed below in the following sequence: (1) dielectric permittivity and loss, (2) average relaxation time, (3) shape of the relaxation spectra, and (4) relaxation strength.

(b1) Dielectric Permittivity and Loss. Results for the OGP nanocomposites are described first. In Figure 7, we show dielectric loss in the frequency domain at −50 °C for PPO2K and OGP2K at four different OG concentrations ($N = 2, 1, 0.5, 0.25$). The segmental and normal mode processes observed in the neat PPO are also seen in the OGP nanocomposites. With decreasing N (increasing OG concentration), both processes shift to higher frequency. This phenomenon was also observed in OGP4K and OGP8K nanocomposites.

Results for the OCP nanocomposites are shown in Figure 8, which describes dielectric loss in the frequency domain at −60 °C for PPO2K and OCP2K ($N = 1$ and 0.5). Here, too, segmental and normal mode processes shift to higher frequency with increasing concentration. An additional high-frequency relaxation due to the β process of OC is also observed. Although the time scale of the segmental motions in OCP nanocomposites measured by DRS decreases slightly with increasing OC concentration, the change in glass transition temperature is undetectable by DSC. We ascribe this to the inherent difference in sensitivity between dielectric and calorimetric techniques.

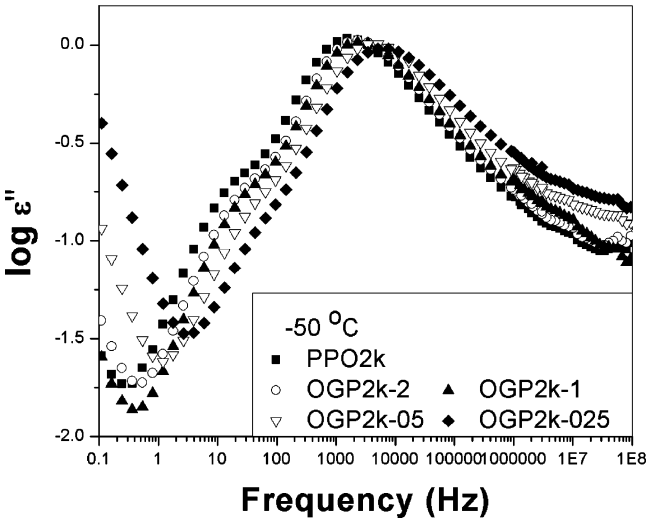

Figure 7. Dielectric loss in the frequency domain with OG concentration as a parameter for OGP2K at 223 K (−50 °C).

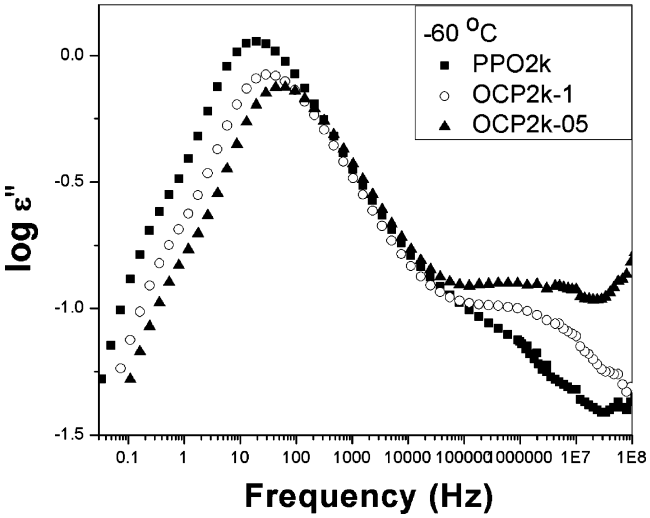

Figure 8. Dielectric loss in the frequency domain with OC concentration as a parameter for OCP2K at 213 K (−60 °C).

The observed variation in the time scale of segmental and normal mode relaxation with composition is of interest. To that

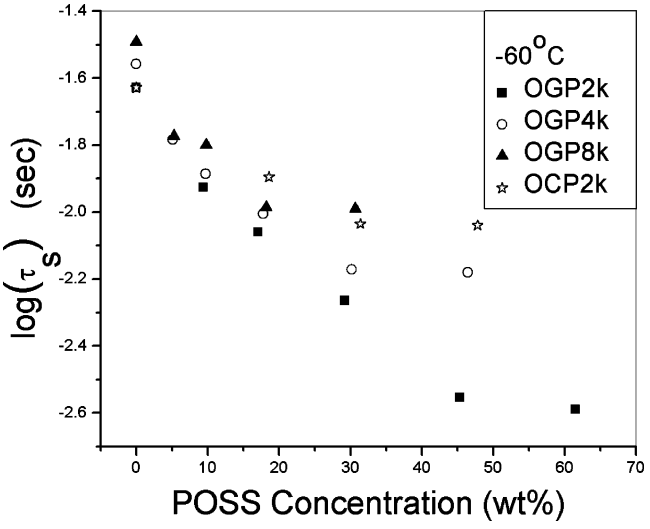

Figure 9. Average relaxation time for segmental process in OGP2K, OGP4K, OGP8K, and OCP2K nanocomposites as a function of POSS concentration at −60 °C.

end a quantitative comparison was made of the experimentally obtained spectra of the neat PPO and POSS/PPO nanocomposites, and the calculated prediction was based upon the rule of mixtures. For the segmental process, the calculated spectrum for OGP shifts to higher frequency with respect to the neat PPO due to the partial overlap with the α process in OG. Interestingly, the experimentally measured spectrum shifts to still higher frequency. This suggests that the shift of the segmental process in OGP nanocomposites stems not only from the overlapping α processes but also from the interactions between OG and PPO. The calculated spectrum of OCP does not shift to higher frequency with respect to the neat PPO, but the measured spectrum does. This indicates that the shift of the segmental process in OCP derives only from the interactions between OC and PPO. For the normal mode process, the calculated spectra of OGP and OCP do not shift with respect to the neat PPO4K, but the measured spectra do. The normal mode process in nanocomposites is affected only by the interactions between POSS nanoparticles and PPO.

In sum, the dynamics of OGP and OCP nanocomposites are affected by the POSS−polymer interactions and cannot be predicted by a simple rule of mixtures. It is likely that POSS nanoparticles act as hard-sphere diluents in the polymer matrix, decreasing the self-association interactions and promoting motions of polymer chains. Additionally, POSS nanoparticles in OGP8K and OCP8K nanocomposites may affect the entanglements (MW for entanglements is 5 kg/mol) and thus contribute to higher mobility.[67,72,73]

(b2) Average Relaxation Time. The average relaxation time for the segmental process in OGP2K, OGP4K, OGP8K, and OCP2K nanocomposites as a function of POSS concentration at −60 °C is shown in Figure 9.

OGP nanocomposites are considered first. The relaxation time (τ_S) for the segmental process decreases with increasing POSS concentration at a given temperature before leveling off. The observed threshold value for OGP nanocomposites is $N = 0.25$, which corresponds to 45 wt % in OGP2K, 30 wt % in OGP4K, and 18 wt % in OGP8K. The trend of decrease of relaxation time is smaller in higher molecular weight PPO matrix, which is attributed to an increased tendency of OG nanoparticles to form aggregates. We define $\Delta\tau_S$ as the difference between the segmental relaxation time in a nanocomposite and the corresponding neat PPO at the same temperature. The increase in $\Delta\tau_S$ with decreasing temperature signifies that OG has a more pronounced effect on PPO dynamics at lower temperature.

OCP nanocomposites show similar trends as OGP nanocomposites with varying POSS concentration and PPO molecular weight. A comparison of the time scale for segmental motions in OCP and OGP nanocomposites (Figure 9) shows that $\Delta\tau_S$ is less pronounced in the former. We note a threshold value of $N = 0.5$ in OCP nanocomposites (31 wt % in OCP2K, 19 wt % in OCP4K, and 11 wt % in OCP8K), beyond which there is no further effect of concentration on the dielectric response. The larger $\Delta\tau_S$ and the smaller threshold value of N in OGP nanocomposites are the consequence of a better dispersion of OG in the PPO matrix and the overlap of their segmental processes.

The average relaxation time for the normal mode process follows a trend similar to that observed for the segmental process with varying POSS concentration and temperature in both OGP and OCP nanocomposites.

POSS nanoparticles decrease the self-association interactions and promote motions of polymer chains. This effect varies with the nanoparticle surface area and is concentration-dependent. At low concentration POSS is well dispersed, the total surface area of nanoparticles increases with concentration and the time scale of relaxation speeds up. At the solubility limit, the interplay sets in between an increase in the surface area due to the additional POSS nanoparticles and a decrease in the effective surface area due to aggregation. This is accompanied by leveling off of the relaxation rate.

The temperature dependence of the relaxation time for segmental (τ_S) and normal (τ_N) processes was fitted with the VFT equation,[66,67] as shown in Figure 13. We observe that the temperature dependence of the average relaxation times becomes gradually less pronounced (decreasing curvature) with increasing POSS concentration. This trend can be rationalized on the basis of intermolecular cooperativity. Since POSS nanoparticles decrease the self-association interactions within the polymer matrix, it is plausible that the cooperative dynamics of PPO evolve toward a weaker intermolecular coupling with increasing POSS concentration. This is tantamount to saying that the fragility of nanocomposites decreases with increasing POSS concentration.

(b3) Relaxation Spectra. The spectral analysis using the HN functional form yielded interesting results. The effects of POSS type and concentration, PPO molecular weight, and temperature on the spectral shape were examined, and the following observations were made. First, the spectra for the segmental process broaden with increasing POSS concentration. The HN parameter *a*, which defines the spectral breadth, decreases from 0.95 to 0.80 for OGP and from 0.95 to 0.86 for OCP, while the HN parameter *b*, which defines the spectral symmetry, remains unchanged. The HN parameters for the normal mode process did not change. The best fits were obtained by setting the HN parameter $b = 1$, which reduces the HN equation to the Cole−Cole (CC) equation. Second, the effect of POSS concentration on the shape of the spectrum becomes less pronounced at higher PPO molecular weight. And third, the normalized loss spectra (not shown here) indicate that segmental and normal mode processes remain thermodielectrically simple over a wide range of temperature at a given POSS concentration.

(b4) Relaxation Strength. The effect of POSS concentration on the dielectric relaxation strength ($\Delta\epsilon$) in OGP and OCP nanocomposites is described next. $\Delta\epsilon$ is an important material characteristic because it depends on the chemical structure and

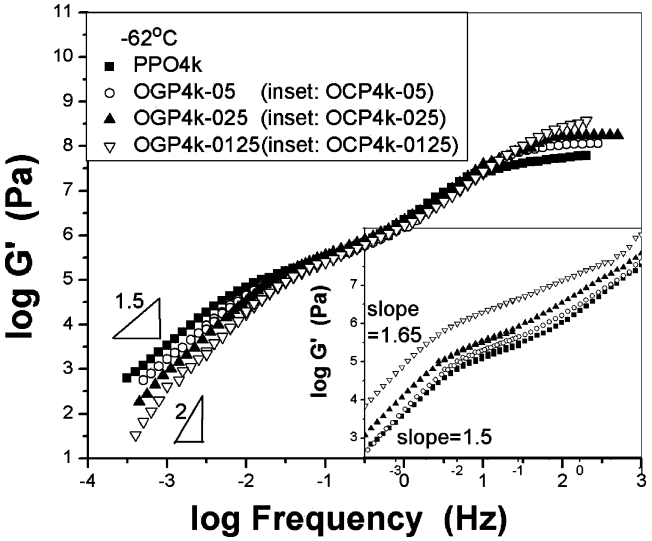

Figure 10. Storage modulus (G') of OGP4K and OCP4K (inset) in the frequency domain at 211 K (−62 °C) with POSS concentration as a parameter. The curves were shifted horizontally using data at 211 K (−62 °C) as reference.

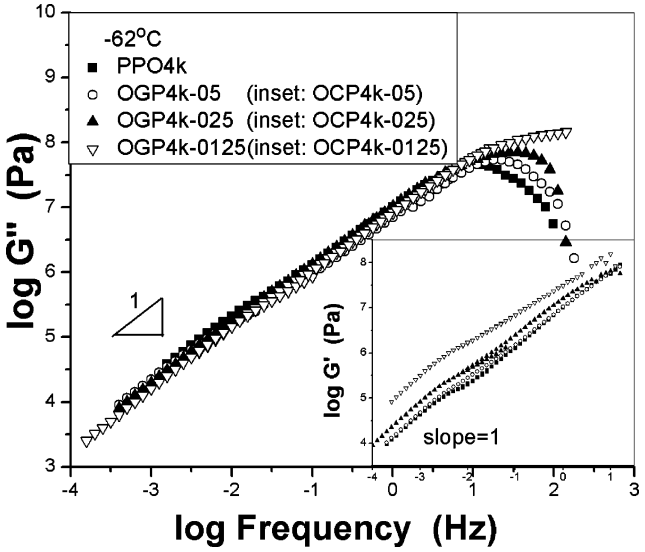

Figure 11. Loss modulus (G'') of OGP4K and OCP4K (inset) in the frequency domain at 211 K (−62 °C) with POSS concentration as a parameter. The curves were shifted horizontally using data at 211 K (−62 °C) as reference.

molecular architecture. The relaxation strength is defined as $\Delta\epsilon = \epsilon'_0 - \epsilon'_\infty$, where ϵ'_0 and ϵ'_∞ represent the limiting low- and high-frequency dielectric permittivity for a given process, respectively, and is proportional to the concentration of dipoles and the mean-squared dipole moment per molecule. The values of $\Delta\epsilon$ are obtained from the HN fits of dielectric spectra. The dielectric relaxation strength of the segmental process ($\Delta\epsilon_S$) increases with increasing POSS concentration in OGP nanocomposites and decreases in OCP nanocomposites. The increase of $\Delta\epsilon_S$ in OGP nanocomposites is caused by the overlap of segmental processes in OG and PPO. Conversely, $\Delta\epsilon_S$ decreases with increasing OC concentration (and approaches zero at 100 wt % OC) in OCP nanocomposites where the sole contribution to the segmental process comes from PPO. The dielectric relaxation strength of the normal mode process ($\Delta\epsilon_N$) is a very weak (decreasing) function of POSS concentration in both OGP and OCP nanocomposites. This is not surprising because the normal mode relaxation is due solely to the PPO chains.

(c) Dynamic Mechanical Spectroscopy (DMS). The results of dynamic mechanical spectroscopy (DMS) are discussed next. We present only the data for OGP and OCP nanocomposites with the PPO4K matrix because analogous results were observed in samples with different PPO molecular weight. The storage modulus in the frequency domain for neat PPO4K, OGP4K, and OCP4K (inset) at −62 °C with POSS concentration as a parameter is shown in Figure 10. Data shown in Figures 10 and 11 were shifted with respect to the reference curve at −62 °C. Figure 10 shows how variation in POSS concentration affects the viscoelastic response in segmental and terminal zones of OGP and OCP (inset) nanocomposites. Terminal relaxation in OGP nanocomposites shifts to higher frequency, and the slope increases from 1.5 to 2.0 with increasing OG concentration. The plateau modulus (G_N) was determined from Figure 10 by taking the value of the onset of transition from segmental to terminal relaxation. G_N in the OGP nanocomposites is not a function of OG concentration and has the same value as in the neat PPO. The thus obtained value of 7×10^5 Pa was used in the subsequent calculation of the average relaxation time for the normal mode process. The experimental results for OCP nanocomposites at higher frequency, which are determined from the experimental data at lower temperature, are not shown here because samples become brittle and difficult to measure. The G_N in OCP nanocomposites increases gradually with increasing OC concentration at 211 K, as seen in the inset of Figure 10. The slope of the terminal region of OCP nanocomposites is a weak function of OC concentration and increases from 1.5 to 1.65 with increasing concentration. Our results show that both OGP and OCP nanocomposites become more liquidlike with incorporation of POSS nanoparticles, although this effect is notably weaker in OCP.

A comparison of the loss modulus spectra for OGP and OCP nanocomposites is presented in Figure 11, which shows loss modulus (G'') in the frequency domain for OGP4K and OCP4K (inset) at −62 °C with POSS concentration as a parameter. The slope in the terminal zone equals 1 and does not vary with POSS concentration in OGP or OCP nanocomposites. The time scale of the segmental process in OGP, located at the high-frequency end, decreases with increasing OG concentration. The speeding up of the segmental process has been attributed to the effect of POSS nanoparticles which decrease the self-association interactions and promote motions of polymer segments. G'' of OCP nanocomposites increases with increasing OC concentration. The observed increase in G' and G'' in OCP nanocomposites could be caused by the "filler effect"[74,75] which is indicative of the interactions between the OC aggregates and the PPO chains. Individual polymer molecules can adopt stretched configurations that promote the adsorption on the surface of OC aggregates due to enhanced polymer−particle interactions.[76] The filler effect is more pronounced in OCP nanocomposites because of the OC crystals, while OG is a viscous liquid.

Zero-shear viscosity (η_0) of nanocomposites, plotted in Figure 12, was extracted directly from the data by averaging the low shear rate values of η. Identical results were obtained by calculating the zero-shear viscosity from $\eta_0 = \lim\{G''(\omega)/\omega\}$ as $\omega \rightarrow 0$. Figure 12 shows η_0 for OGP4K and OCP4K (inset) nanocomposites as a function of POSS concentration at 273 K. An increase in POSS concentration leads to a decrease in η_0 in OGP nanocomposites and an increase in OCP nanocomposites. Zero-shear viscosity of the OGP nanocomposites obeys the rule of mixtures and exhibits a constant slope of −3.9. This is very different from OCP nanocomposites, shown in the inset in Figure 12. The dash line in the inset is calculated from the theory of hard-sphere-filled suspensions.[77−79] It is apparent that the

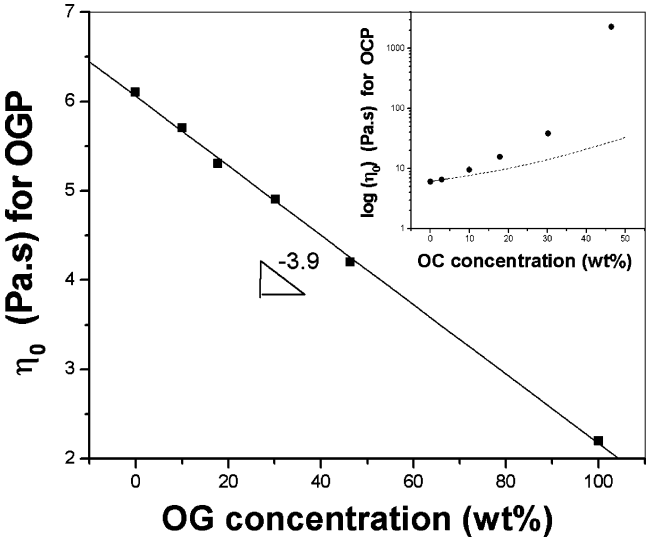

Figure 12. Zero-shear viscosity of OGP and OCP (inset) nanocomposites as a function of POSS concentration at 273 K.

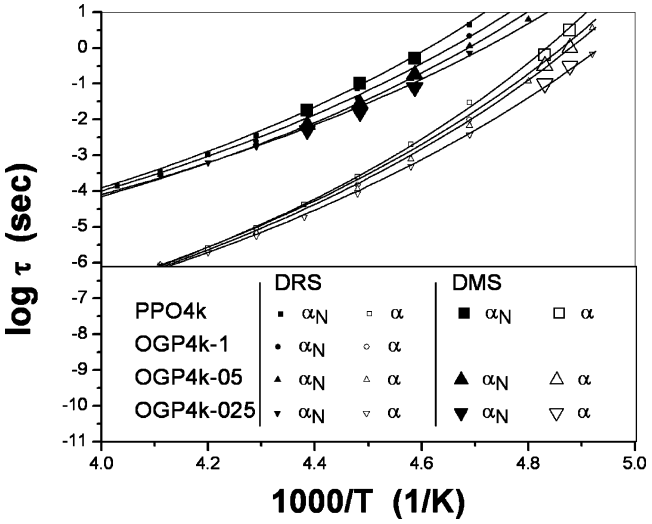

Figure 13. Average DMS and DRS relaxation time for segmental (open symbols) and normal mode (solid symbols) processes in neat PPO4K and OGP4K as a function of reciprocal temperature with POSS concentration as a parameter. Large symbols are DMS results, and small symbols are DRS results. The solid lines are fits to the VFT equation.

viscosity of OCP nanocomposites does not obey this theory and exhibits a higher value instead. The reason for this effect lies in the strong PPO−OC interactions that impart a solidlike behavior to OCP nanocomposites.

The combined results of DRS and DMS analysis are displayed in Figure 13, which represents a composite plot of the average relaxation time for the segmental and normal mode process in OGP4K as a function of temperature and OG concentration. The solid lines are fits to the VFT equation. The average DRS relaxation times for segmental and normal mode processes were obtained from the HN fits. The average DMS relaxation time for the segmental process was determined from $\tau_S = 1/\omega_{max} = 1/(2\pi f_{max})$, and the average DMS relaxation time for the normal mode process, τ_N, was calculated from[80]

$$\tau_N \equiv \frac{\eta_0}{G_N} = \frac{\sum_p \tau_{G,p} h_p}{\sum_p h_p} \quad (4)$$

where $\tau_{G,p}$ and h_p are the relaxation time and the intensity for the pth viscoelastic relaxation mode. The relaxation time is calculated from experimentally determined zero-shear viscosity (η_0) and plateau modulus (G_N). To afford a direct comparison of τ_N obtained from DRS and DMS data, we had to divide the DMS τ_N by two. This is because the longest viscoelastic relaxation time (τ_{N1DMS}) of the Rouse chain is one-half the longest dielectric relaxation time (τ_{N1DRS}) and twice that of the second dielectric normal mode (τ_{N2DRS}), which is experimentally measured in samples with symmetrically inverted dipoles. Hence, $\tau_{N1DMS} = {}^1/_2\tau_{N1DRS} = 2\tau_{N2DRS}$. A comparative analysis of DRS and DMS yields the following key observations: (1) the average relaxation times for segmental and normal mode processes obtained from DMS and DRS data follow the same general trend with temperature and POSS concentration, and (2) the time scales of the segmental and normal mode process obtained from DRS and DMS are in excellent agreement.

Conclusion

We have completed an investigation of the dynamics of multifunctional POSS/PPO nanocomposites. Three PPOs of different molecular weight and two multifunctional POSS reagents, octaglycidyldimethylsilyl-POSS (OG) and octaepoxycyclohexyldimethylsilyl-POSS (OC), were used to prepare the samples. Dynamics of neat PPO, OG, OC, and POSS/PPO nanocomposites were investigated over a broad range of frequency and temperature using dielectric relaxation spectroscopy (DRS) and dynamic mechanical spectroscopy (DMS).

Segmental (α) and normal mode (α_N) processes in PPO are in excellent agreement with the results reported in the literature. Neat OG and OC also display two relaxation processes: a slower one due to the segmental motions of side chains and a faster one due to the local motions. OC dynamics are characterized by a longer time scale than OG because of the increased rigidity of side chains due to the incorporation of the cyclohexyl ring and a higher T_g.

All nanocomposites show segmental and normal mode processes that shift to higher frequency with increasing POSS concentration. POSS nanoparticles act as hard-sphere diluents in the polymer matrix that trigger a decrease in self-association interactions among the PPO chains and thus promote their mobility. Good dispersion of POSS is limited by aggregation at higher concentration. We defined $\Delta\tau$ as the difference between the average relaxation time of the a process (segmental and normal mode) in a nanocomposite and the corresponding neat PPO at the same temperature. $\Delta\tau$ is affected by the structure and concentration of POSS and PPO molecular weight and temperature as follows: (1) $\Delta\tau$ increases gradually with increasing POSS concentration before leveling off at a threshold value due to POSS aggregation, (2) $\Delta\tau$ decreases with increasing PPO molecular weight, (3) $\Delta\tau$ increases with decreasing temperature, and (4) $\Delta\tau$ is greater in OGP than OCP nanocomposites under the same conditions.

A change in temperature does not affect the shape of the relaxation spectra of segmental and normal mode processes; i.e., they remain thermodielectrically simple. An increase in POSS concentration, however, leads to a slight broadening of the segmental process but does not change the shape of the normal mode process. The effect of POSS concentration on the segmental relaxation spectra decreases with increasing molecular weight of PPO, which is attributed to an increased tendency of POSS nanoparticles to form aggregates in a higher molecular weight matrix.

The dielectric strength of the segmental process in OGP nanocomposites increases with increasing OG concentration because of the partial overlap of segmental relaxations in OG and PPO. Conversely, the dielectric strength of the segmental process in OCP nanocomposites derives from the PPO segments only and decreases with increasing OC concentration. The dielectric strength of the normal mode process decreases with increasing POSS concentration in all nanocomposites. This is not surprising because that relaxation is due solely to the global motion of PPO chains.

A direct comparison of DRS and DMS results reveals excellent agreement between the average relaxation time for segmental and normal mode process obtained by those two techniques. The plateau modulus (G_N) does not change with increasing POSS concentration in the OGP nanocomposites but increases in the OCP nanocomposites. The observed increase in the modulus and viscosity of OCP nanocomposites may be attributed to the "filler effect" and the presence of OC crystalline phase.

Acknowledgment. This work is supported by National Science Foundation under Grant DMR-0346435.

References and Notes

(1) Whitesides, G. M.; Mathias, T. P.; Seto, C. T. *Science* **1991**, *254*, 1312.
(2) Krishnamoorti, R.; Vaia, R. A. *Polymer Nanocomposites*; American Chemical Society: Washington, DC, 2003.
(3) Nalwa, H. S. *Handbook of Organic-Inorganic Hybrid Materials and Nanocomposites*; American Scientific Publishers: Stevenson Ranch, CA, 2003; Vol. 2.
(4) Pielichowski, K.; Njuguna, J.; Janowski, B.; Pielichowski, J. *Adv. Polym. Sci.* **2006**, *201*, 225.
(5) Lichtenhan, J. D.; Vu, N. Q.; Carter, J. A.; Gilman, J. W.; Feher, F. J. *Macromolecules* **1993**, *26*, 2141.
(6) Lichtenhan, J. D. *Polymeric Materials Encyclopedia*; CRC Press: New York, 1996.
(7) Schwab, J. J.; Lichtenhan, J. D. *Appl. Organomet. Chem.* **1998**, *12*, 707.
(8) Lucke, S.; Stoppek-Langner, K. *Appl. Surf. Sci.* **1999**, *145*.
(9) Li, G. Z.; Wang, L. C.; Ni, H. L.; Pittman, C. U. *J. Inorg. Organomet. Polym.* **2001**, *11*, 123.
(10) Fu, B. X.; Hsiao, B. S.; Pagola, S.; Stephens, P.; White, H.; Rafailovich, M.; Sokolov, J.; Mather, P. T.; Jeon, H. G.; Phillips, S.; Lichtenhan, J. D.; Schwab, J. J. *Polymer* **2001**, *42*, 599.
(11) Fu, B. X.; Yang, L.; Somani, R. H.; Zong, S. X.; Hsiao, B. S.; Phillips, S.; Blanski, R.; Ruth, P. *J. Polym. Sci., Part B: Polym. Phys.* **2001**, *39*, 2727.
(12) Xu, H. Y.; Kuo, S. W.; Lee, J. S.; Chang, F. C. *Polymer* **2002**, *43*, 5117.
(13) Blanski, R. L.; Phillips, S. H.; Chaffee, K. P.; Lichtenhan, J. D.; Lee, A.; Geng, H. P. *Polym. Prepr.* **2000**, *41*, 585.
(14) Waddon, A. J.; Zheng, L.; Farris, R. J.; Coughlin, E. B. *Nano Lett.* **2002**, *2*, 1149.
(15) Lee, A.; Lichtenhan, J. D. *Macromolecules* **1998**, *31*, 4970.
(16) Lee, A.; Lichtenhan, J. D. *J. Appl. Polym. Sci.* **1999**, *73*, 1993.
(17) Lichtenhan, J. D.; Otonari, Y. A.; Carr, M. J. *Macromolecules* **1995**, *28*, 8435.
(18) Zheng, L.; Waddon, A. J.; Farris, R. J.; Coughlin, E. B. *Macromolecules* **2002**, *35*, 2375.
(19) Lichtenhan, J. D.; Noel, C. J.; Bolf, A. G.; Ruth, P. N. *Mater. Res. Soc. Symp. Proc.* **1996**, *435*, 3.
(20) Lichtenhan, J. D. *Comments Inorg. Chem.* **1995**, *17*, 115.
(21) Fu, B. X.; Hsiao, B. S.; Pagola, S.; Stephens, P.; White, H.; Rafailovich, M.; Mather, P. t.; Jeon, H. G.; Phillips, S.; Lichtenhan, J. D.; Schwab, J. J. *J. Polymer* **2000**, *45*, 599.
(22) Haddad, T. S.; Lichtenhan, J. D. *Macromolecules* **1996**, *29*, 7302.
(23) Mather, P. T.; Jeon, H. G.; Romo-Uribe, A.; Haddad, T. S.; Lichtenhan, J. D. *Macromolecules* **1998**, *32*, 1194.
(24) Zheng, L.; Farris, R. J.; Coughlin, E. B. *Macromolecules* **2001**, *34*, 8034.
(25) Xu, H. Y.; Kuo, S. W.; Lee, J. S.; Chang, F. C. *Macromolecules* **2002**, *35*, 8788.
(26) Xu, H. Y.; Kuo, S. W.; Chang, F. C. *Polym. Bull. (Berlin)* **2002**, *48*, 469.
(27) Schwab, J. J.; Haddad, T. S.; Lichtenhan, J. D.; Mather, P. T.; Chaffee, K. P. *Antek* **1997**, *611*, 1817.
(28) Kopesky, E. T.; Haddad, T. S.; Cohen, R. E.; Mckinley, G. H. *Macromolecules* **2004**, *37*, 8992.
(29) Fu, B. X.; Gelfer, M. Y.; Hsiao, B. S.; Phillips, S.; Viers, B.; Blanski, R. P. R. *Polymer* **2003**, *44*, 1499.
(30) Joshi, M.; Butola, B. S.; Simon, G.; Kukaleva, N. *Macromolecules* **2006**, *39*, 1839.
(31) Capaldi, F. M.; Rutledge, G. C.; Boyce, M. C. *Macromolecules* **2005**, *38*, 6700.
(32) Romo-Uribe, A.; Mather, P. T.; Haddad, T. S.; Lichtenhan, J. D. *J. Polym. Sci., Part B: Polym. Phys.* **1998**, *36*, 1857.
(33) Huang, C.; Kuo, S.; Lin, F.; Huang, W.; Wang, C.; Chen, W.; Chang, F. *Macromolecules* **2006**, *39*, 300.
(34) Liu, H.; Zheng, S.; Nie, K. *Macromolecules* **2005**, *38*, 5088.
(35) Drazkowski, D. B.; Lee, A.; Haddad, T. S.; Cookson, D. J. *Macromolecules* **2006**, *39*, 1854.
(36) Bizet, S.; Galy, J.; Gerard, J. *Macromolecules* **2006**, *39*, 2574.
(37) Tsuchida, A.; Bolln, C.; Sernetz, F. G.; Frey, H.; Mulhaupt, R. *Macromolecules* **1997**, *30*, 2818.
(38) Turri, S.; Levi, M. *Macromolecules* **2005**, *38*, 5569.
(39) Zheng, L.; Hong, S.; Cardoen, G.; Burgaz, E.; Gido, S. P.; Coughlin, E. B. *Macromolecules* **2004**, *37*, 8606.
(40) Liang, K.; Toghiani, H.; Li, G.; Pittman, C. U. *J. Polym. Sci., Part A: Polym. Chem.* **2005**, *43*, 3887.
(41) Li, G.; Cho, H.; Wang, L. C.; Toghiani, H.; Pittman, C. U. *J. Appl. Polym. Sci., Part A: Polym. Chem.* **2005**, *43*, 355.
(42) Li, G.; Thompson, T.; Daulton, T. L.; Pittman, C. U. *Polymer* **2002**, *43*, 4167.
(43) Cho, H.; Liang, K.; Chatterjee, S.; Pittman, C. U. *J. Inorg. Organomet. Polym. Mater.* **2005**, *15*, 541.
(44) Li, G.; Wang, L. C.; Toghiani, H.; Daulton, T. L.; Koyama, K.; Pittman, C. U. *Macromolecules* **2001**, *34*, 8686.
(45) Liang, K.; Li, G.; Toghiani, H.; Koo, J. H.; Pittman, C. U. *Chem. Mater.* **2006**, *18*, 301.
(46) Patel, R. R.; Mohanraj, R.; Pittman, C. U. *J. Polym. Sci., Part B: Polym. Phys.* **2006**, *44*, 234.
(47) Zhang, Y.; Lee, S.; Yoonessi, M.; Liang, K.; Pittman, C. U. *Polymer* **2006**, *47*, 2984.
(48) Chen, W.; Wang, Y.; Kuo, S.; Huang, C.; Tung, P.; Chang, F. *Polymer* **2004**, *45*, 6897.
(49) Choi, J.; Kim, S. G.; Laine, R. M. *Macromolecules* **2004**, *37*, 99.
(50) Choi, J.; Harcup, J.; Yee, A. F.; Zhu, Q.; Laine, R. M. *J. Am. Chem. Soc.* **2001**, *123*, 11420.
(51) Choi, J.; Yee, A. F.; Laine, R. M. *Macromolecules* **2004**, *37*, 3267.
(52) Choi, J.; Tamaki, R.; Kim, S. G.; Laine, R. M. *Chem. Mater.* **2003**, *15*, 3365.
(53) Kim, G. M.; Qin, H.; Fang, X.; Sun, F. C.; Mather, P. T. *J. Polym. Sci., Part B: Polym. Phys.* **2003**, *41*, 3299.
(54) Tamaki, R.; Choi, J.; Laine, R. M. *Chem. Mater.* **2003**, *15*, 793.
(55) Ni, Y.; Zheng, S.; Nie, K. *Polymer* **2004**, *45*, 5557.
(56) Adachi, K.; Kotaka, T. *Prog. Polym. Sci.* **1993**, *18*, 585.
(57) Watanabe, H. *Macromol. Rapid Commun.* **2001**, *22*, 127.
(58) Watanabe, H. *Prog. Polym. Sci.* **1999**, *24*, 1253.
(59) Adachi, K. *Dielectric Spectroscopy of Polymeric Materials*; American Chemical Society: Washington, DC, 1997.
(60) Mijovic, J.; Miura, N.; Monetta, T.; Duan, Y. *Polym. News* **2001**, *26*, 251.
(61) Fitz, B.; Andjelic, S.; Mijovic, J. *Macromolecules* **1997**, *30*, 5227.
(62) Mijovic, J.; Bian, Y.; Gross, R. A.; Chen, B. *Macromolecules* **2005**, *38*, 10812.
(63) Williams, G. Dielectric relaxation spectroscopy of amorphous polymer systems: the modern approches. In *Keynote Lectrues in Selected Topics of Polymer Science*; CSIC: Madrid, 1997.
(64) Williams, G. Theory of dielectric properties. In *Dielectric Spectroscopy of Polymeric Materilas*; American Chemical Society: Washington, DC, 1997.
(65) Kremer, F. *Broadband Dielectric Spectroscopy*; Springer-Verlag: Berlin, 2002.
(66) Mijovic, J.; Han, Y.; Sun, M.; Pejanovic, S. *Macromolecules* **2003**, *36*, 4589.
(67) Mijovic, J.; Sun, M.; Han, Y. *Macromolecules* **2002**, *35*, 6417.
(68) Havriliak, S., Jr.; Negami, S. *Polymer* **1967**, *8*, 161.
(69) Cole, R. H.; Cole, K. S. *J. Chem. Phys.* **1942**, *10*, 98.
(70) Paluch, M.; Roland, C. M.; Gapinski, J.; Patkowski, A. *J. Chem. Phys.* **2003**, *118*, 3177.
(71) Casalini, R.; Livi, A.; Rolla, P.; Levita, G.; Fioretto, D. *Phys. Rev. B* **1996**, *53*, 564.
(72) Nicolai, T.; Floudas, G. *Macromolecules* **1998**, *31*, 2578.
(73) Nicolai, T.; Prochazka, F.; Durand, D. *Phys. Rev. Lett.* **1999**, *82*, 863.

(74) Zhu, Z.; Thompson, T.; Wang, S. Q.; Meerwall, E. D.; Halasa, A. *Macromolecules* **2005**, *38*, 8816.
(75) Mijovic, J.; Lee, H. K.; Kenny, J.; Mays, J. *Macromolecules* **2006**, *39*, 2172.
(76) Zhang, Q.; Archer, L. A. *Langmuir* **2002**, *18*, 10435.
(77) Batchelor, G. K. *J. Fluid Mech.* **1970**, *41*, 545.
(78) Batchelor, G. K. *J. Fluid Mech.* **1971**, *46*, 813.
(79) Batchelor, G. K. *J. Fluid Mech.* **1977**, *83*, 97.
(80) Graessley, W. W. *Adv. Polym. Sci.* **1974**, *16*, 1.

MA0704109